

Optical isotropy in structurally anisotropic halide scintillators: *Ab initio* study

G. Shwetha and V. Kanchana*

*Department of Physics, Indian Institute of Technology Hyderabad, Ordnance Factory Estate,
Yeddumailaram 502 205, Andhra Pradesh, India*

(Received 28 June 2012; revised manuscript received 20 August 2012; published 21 September 2012)

The present study explores the structural, electronic, and optical properties of $XSrI_3$ ($X = K, Rb, \text{ and } Cs$) compounds within the framework of density functional theory. The ground state properties are calculated using the pseudopotential method with the inclusion of van der Waals interactions, which we find inevitable in reproducing the experimental structural properties of the above mentioned compounds with layered crystal structure. The electronic and optical properties are calculated using the full-potential linearized augmented plane wave method and the band structures are plotted with various functionals and we find the newly developed Tran and Blaha modified Becke-Johnson potential to improve the band gap significantly. From the band structures of these compounds, it is clearly seen that $I-p$ states dominate the valence band. The optical properties such as complex dielectric function, refractive index, absorption spectra, and electron energy loss spectra are calculated which clearly reveal the optically isotropic nature of these materials though being structurally anisotropic, which is the key requirement for ceramic scintillators. The present study suggests that among the three compounds studied, $CsSrI_3$ can act as a fast scintillating compound, which is well explained from the band structure calculations.

DOI: [10.1103/PhysRevB.86.115209](https://doi.org/10.1103/PhysRevB.86.115209)

PACS number(s): 63.20.dk, 78.20.Ci, 78.20.Bh, 78.66.Hf

I. INTRODUCTION

Scintillators play a major role in the development of modern physics as they are ideal devices to detect and measure the elementary particles. Scintillators with high light output, quantum efficiency, and high energy resolution can be used as radiation detectors in industrial inspection and in medical diagnostics. The performance of a scintillator can be characterized by its high light output and its propagation characteristics with the excitation energy (proportionality), decay time, density, and energy resolution. Over the past few decades, the scientific research on scintillating materials is focused more towards the discovery of new types of scintillators that fulfill the above said requirements. In general, scintillation phenomena can be observed in materials such as organic and inorganic crystals, fluids, and also in gases. Among these, inorganic solids possess superior scintillating properties such as high efficiency, fast scintillation, and good energy resolution. Inorganic materials, namely $CaWO_4$ and ZnS , are found to be good scintillators to detect and count the radioactivity.¹⁻³ Alkali and alkaline-earth halides have high light output and act as fast luminescence scintillators.⁴⁻⁸ $LaBr_3$ activated with Ce^{3+} is found to be a very high light output proportional scintillator with energy resolution less than 3% at 662 KeV.^{9,10} SrI_2 and Eu^{2+} activated SrI_2 ¹¹⁻¹³ were found to be good ceramic scintillators and were also found suitable for gamma and neutron detection.

Scintillators exhibit fast scintillation mechanisms¹⁴ via core-valence (CV)¹⁵⁻¹⁸ transition (Ba, Cs, Rb based fluorides, chlorides, and bromides), interconfiguration transitions (Ce^{3+} , Pr^{3+} , and Nd^{3+} ions) and exciton, excitonic like luminescence (pure compounds). Halide scintillators of AX , ABX_3 (where $X = F, Cl, Br$ and A, B are single and divalent cations) type were studied and found to exhibit fast scintillation properties.¹⁴ On passing from AX to ABX_3 compounds, the distance between nearest neighboring ions A^+ and X^- ,

which are involved in the CV transition increases and as a result the probability of CV transitions become smaller and decay time, light output (slightly) increases.^{14,16,19} Among the pure and doped ABX_3 type compounds, $LiBaF_3$, $KMgF_3$ ²⁰⁻²³ were used as scintillator detectors and thermoluminescent dosimeters. Core valence transitions are observed in $CsMgCl_3$, $CsSrCl_3$,²⁴ and $RbCaF_3$ ²⁵ compounds and they also show short decay time and high emission intensity at room temperature. Multiple spontaneous emissions were predicted in Yb^{2+} doped $CsCaBr_3$ through *ab initio* quantum chemical calculations.²⁶

The scintillation phenomena can occur in various ways depending on the type of transitions involved. The compounds like BaF_2 and CsF are found to be fast scintillators due to the radiative transition of electrons from halogen derived valence band to the next deeper metal derived core valence states and these types of transitions are called Auger-free luminescence or core-valence luminescence. The compounds which exhibit CV luminescence are called L -type because of $E_g > E_{vc}$ where E_g is the energy gap between valence band and conduction band and E_{vc} is the energy difference between the top of the valence band to the top of the core valence band. In the case of compounds like SrI_2 and CaF_2 the transition is observed from conduction band to valence band and is called Auger luminescence. These compounds (SrI_2 , CaF_2) are referred to as A -type where $E_g < E_{vc}$, whereas in the case of CsI , $E_g > E_{vc} - \Delta E_v$, where ΔE_v is the width of the valence band and it is called AL -type and they exhibit fast scintillation.

In this present work, we aim to understand the type of transition involved in the inorganic halide scintillators $XSrI_3$ where $X = K, Rb, \text{ and } Cs$ through electronic band structure calculations. The other objective of the present work is to understand the effect of van der Waals interactions on crystal binding and its effect on other physical properties. The organization of the paper is as follows. In Sec. II we

have presented the computational details of the present work. Section III deals with the results and discussions and at the end we have given a brief conclusion of the present study.

II. COMPUTATIONAL DETAILS

We have performed geometry optimization with Cambridge Series of Total Energy Package (CASTEP) code^{27–29} using Vanderbilt-type ultrasoft pseudopotentials.³⁰ The plane wave cutoff energy of 430 eV and $6 \times 6 \times 2$ k mesh was used to achieve reasonable convergence. The sampling integration over the Brillouin zone was employed by using Monkhorst-Pack³¹ method. The exchange-correlation potential of Ceperley and Alder³² parametrized by Perdew and Zunger³³ in the local density approximation and the generalized gradient approximation with the Perdew-Wang (PW91)³⁴ parametrization were used. The structure parameters were calculated by using the Broyden, Fletcher, Goldfarb, and Shannon (BFGS) minimization technique.³⁵ All the three studied compounds crystallize in the orthorhombic structure with space group $Cmcm(63)$. The experimental atomic positions of $CsSrI_3$ compound are used for optimizing the position of the remaining compounds due to the lack of experimental data. We have taken the experimental lattice parameters as an initial step for the geometry optimization using the various exchange-correlation functionals available. Since the present materials have layered crystal structure, the van der Waals (vdW) interactions would play a dominant role on the physical and chemical properties. We have also included these vdW interactions by means of semiempirical dispersion corrected density functional theory as implemented in CASTEP code. In this semiempirical dispersion corrected DFT (DFT-D),^{36–42} the long range interactions are approximated by a simple long range potential $f_{ij}(R) \cdot C_{6,ij} \cdot R_{ij}^{-6}$, where $C_{6,ij}$ is the dispersion coefficient between any atom pair i and j at a distance R_{ij} and $f_{i,j}(R)$ is the damping function which is equal to zero for smaller values of R_{ij} (short range) and one for larger values of R_{ij} . The calculated dispersion coefficients $C_{6,ij}$ are 6.132×10^3 , 7.009×10^3 , 1.031×10^4 , 3.254×10^3 , 2.244×10^2 eV \AA^6 and vdW radii R_{ij}^0 are 3.92, 4.22, 4.50, 3.84, and 2.66 \AA for K, Rb, Cs, Sr, and I, respectively.

For computing the electronic and optical properties of the above mentioned compounds, we have employed the full-potential linearized augmented plane wave (FP-LAPW) plus local orbital method as implemented in the WIEN2k^{43,44} package. We have relaxed the internal atomic positions by using the Perdew-Burke-Ernzerhof generalized gradient approximation for the exchange-correlation functional (Table I). In order to relax the atomic positions, we have considered the experimental lattice parameters as input, and then optimized the atomic positions by minimizing the forces on atoms, i.e., forces on all the atoms are almost equal to zero. Once the forces are minimized, one can find the self-consistent density at these positions by turning off the relaxations and driving the system to be self-consistent. We have used $11 \times 11 \times 4$ k mesh in the Brillouin zone (BZ) for the self consistent calculation with $R_{MT}K_{max} = 7$, where R_{MT} is the smallest of all atomic sphere radii and K_{max} is the plane wave cutoff. We have

TABLE I. Optimized internal atomic positions from total energy minimization using FP-LAPW.

	KSrI ₃	RbSrI ₃	CsSrI ₃
X x	0.0000	0.0000	0.0000
X y	0.7489	0.7479	0.7477
X z	0.2500	0.2500	0.2500
Sr x	0.0000	0.0000	0.0000
Sr y	0.0000	0.0000	0.0000
Sr z	0.0000	0.0000	0.0000
I_1 x	0.0000	0.0000	0.0000
I_1 y	0.3587	0.3589	0.3615
I_1 z	0.0600	0.0535	0.0489
I_2 x	0.0000	0.0000	0.0000
I_2 y	0.0821	0.0711	0.0592
I_2 z	0.2500	0.2500	0.2500

used Perdew-Burke-Ernzerhof (PBE),⁴⁵ Engel-Vosko (EV),⁴⁶ and Tran and Blaha modified Becke-Johnson potential (TB-mBJ)^{47–50} functionals for calculating the electronic properties and TB-mBJ alone for calculating the optical properties because of the improved band gap. The EV functional is obtained by optimizing the exchange-correlation potential V_{ex} instead of the energy E_{ex} , and was designed to reproduce the exact band gaps rather than total energy. TB-mBJ is a newly developed semilocal exchange-correlation functional which uses information from kinetic energy density in addition to the charge density as employed in standard GGA. These functionals come in the framework of KS formalism and they are computationally less expensive compared to hybrid functionals. The TB-mBJ functionals cannot be used for total energy calculations but yield improved band gaps in wide variety of materials.^{4,5,47–50}

III. RESULTS AND DISCUSSION

A. Structural properties

The $XSrI_3$ ($X = K, Rb,$ and Cs) compounds are found to have layered structure as shown for $CsSrI_3$ in Fig. 1.

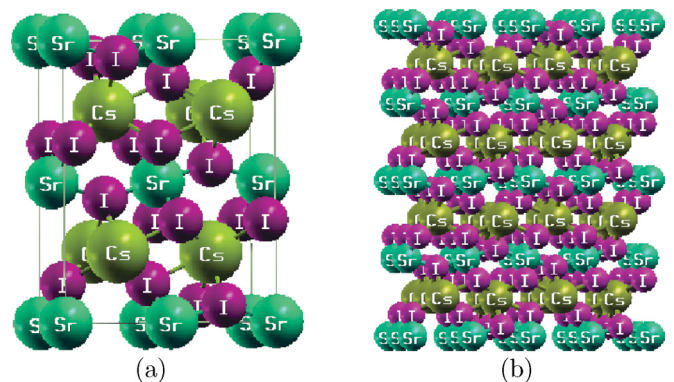


FIG. 1. (Color online) (a) Crystal structure of $CsSrI_3$ compound. (b) Layered crystal structure of $CsSrI_3$ compound. In order to show the layered structure clearly we have presented the supercell structure with an increase in the radius of the elements.

TABLE II. Experimental and optimized lattice parameters, equilibrium volume of KSrI_3 , RbSrI_3 , and CsSrI_3 compounds with LDA, PW91 exchange-correlation functionals, and with OBS dispersion correction method.

		KSrI_3	RbSrI_3	CsSrI_3
LDA	a(Å)	4.56	4.62	4.68
	b(Å)	14.76	14.99	15.08
	c(Å)	11.59	11.78	12.14
	volume(Å ³)	779.81	816.79	856.96
GGA-PW91	a(Å)	4.75	4.86	4.81
	b(Å)	15.65	16.067	16.780
	c(Å)	12.07	12.21	12.31
	volume(Å ³)	897.07	952.30	1009.97
GGA-PW91 + OBS	a(Å)	4.72	4.78	4.86
	b(Å)	15.38	15.58	16.10
	c(Å)	11.97	12.14	12.31
	volume(Å ³)	868.25	903.21	964.16
Expt. ⁵⁶	a(Å)	4.72	4.77	4.82
	b(Å)	15.35	15.55	15.78
	c(Å)	11.94	12.10	12.58
	volume(Å ³)	865.03	896.89	955.95

We have performed full geometry optimization including lattice parameters and atomic positions with the usual DFT exchange-correlation functionals using CASTEP code. We found a large discrepancy between the theory and experimental volume, which may be due to the inadequacy of normal DFT calculations to capture the van der Waals effects in these systems. Hence we employed the DFT-D method to the crystal and relaxed it leading to comparable results with the experiments. However, some of the DFT-D methods (Grimme, TS) are not yet implemented in CASTEP code for the elements (like Cs, Ba, Tl, Pb, Bi, etc.) of 6th, 7th periods of the Periodic Table in CASTEP code. Therefore, in the present

TABLE III. Calculated band gap of XSrI_3 ($X = \text{K, Rb, Sr}$) compounds in eV using different functionals.

	KSrI_3	RbSrI_3	CsSrI_3
PBE	3.81	3.86	3.84
EV	4.42	4.43	4.38
TB-mBJ	4.74	4.80	4.79

study, we have performed full structural optimization using the available GGA-PW91 + OBS method for XSrI_3 ($X = \text{K, Rb, and Cs}$) compounds to account for the vdW interactions and the calculated ground state properties of these compounds with this correction are in excellent agreement with experiment in contrast to the standard LDA and GGA functionals. The lattice parameters, equilibrium volume of these compounds with different exchange-correlation functionals, and dispersion correction are given in Table II and it clearly indicates that the inclusion of van der Waals interactions improves the results significantly.

B. Electronic properties

The band structure of $X(X = \text{K, Rb, Cs})\text{SrI}_3$ compounds (at experimental lattice constant) is calculated using three functionals (PBE, EV, and TB-mBJ) and the band structure using TB-mBJ alone is shown in Fig. 2, and the corresponding band gaps are reported in Table III (for three functionals). From the table, we could find that TB-mBJ values are improved when compared to LDA/GGA. The TB-mBJ functional improves the band gap compared to PBE, EV functionals which is clearly seen from the density of states (DOS) plots also, where we have shown the DOS for all the three functionals in Fig. 3. All the compounds under study are found to be insulators with an indirect band gap between valence band maximum (VBM) at

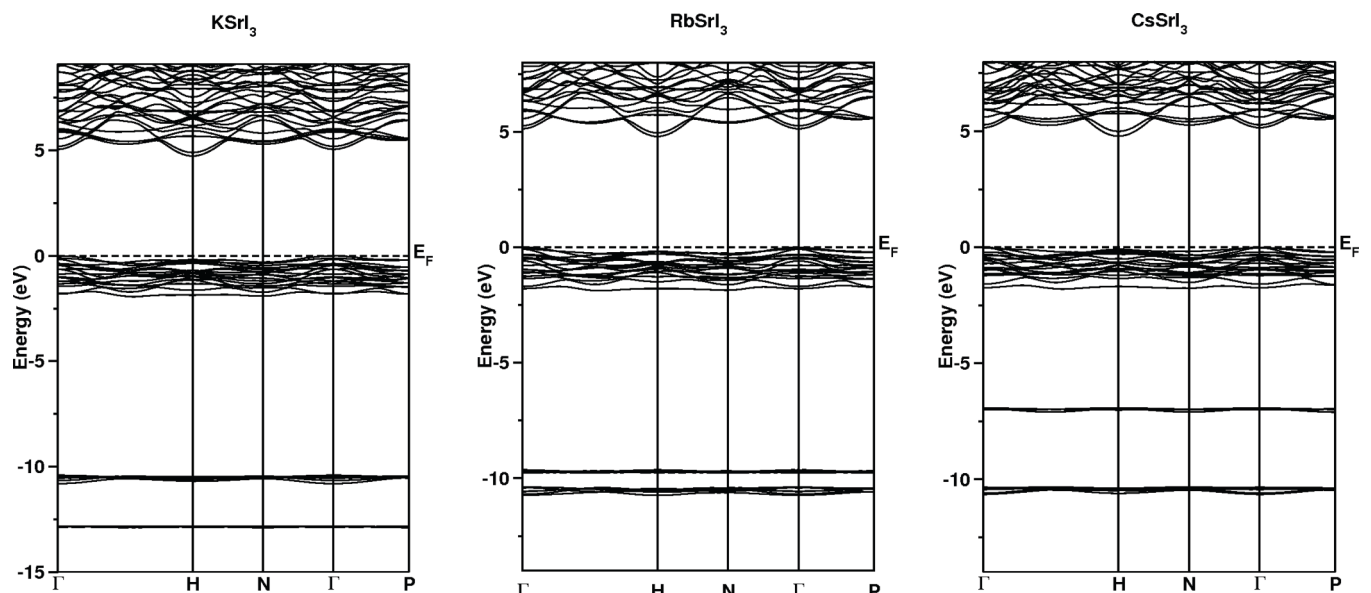


FIG. 2. Band structure of KSrI_3 , RbSrI_3 , and CsSrI_3 along the high symmetry directions using TB-mBJ functional.

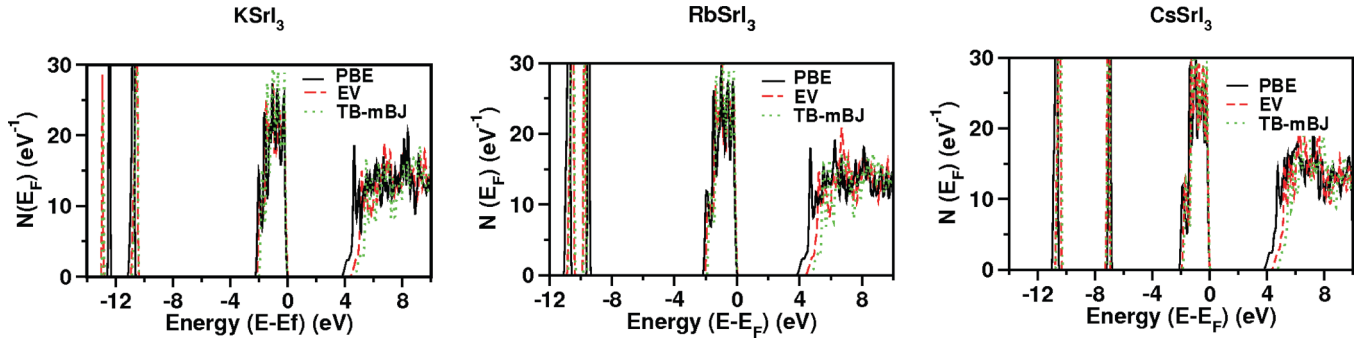


FIG. 3. (Color online) Density of states for KSrI_3 , RbSrI_3 , and CsSrI_3 as calculated with the PBE, EV, and TB-mBJ functionals. The Fermi level is shifted to zero.

Γ point and the conduction band minimum (CBM) at H point (Fig. 2).

The valence band of $X\text{SrI}_3$ ($X = \text{K}, \text{Rb}, \text{Cs}$) compounds contains three regions (from the density of states) as shown in Fig. 4: bottom most, middle, and top of the valence band. For KSrI_3 [Fig. 4(a)], the bottom most valence band below the Fermi level spread around -12.9 to -12.7 eV dominated mostly by K- p like states. The middle of the valence region extending around -10.8 to -10.38 eV are mainly from the I- s like states hybridized with Sr- p and K- p like states. The region near the Fermi level, i.e., top of the valence band spread around -2 to 0 eV have predominantly I- p like character with very less contribution from the Sr- d and p states. In the case of RbSrI_3 , the bottom most, middle, and top of the valence bands spread around -10.83 to 10.31 eV, -9.8 to -9.5 eV, and -2 to 0 eV, respectively. The bottom region is dominated by the I- s states hybridized with the Rb- p and Sr- p states, whereas the middle region is dominated by Rb- p like states with less contribution from the I- s states. The contribution for the top of the valence band region is mainly from the hybridization of I- p , Sr- d , p , and s states.

For CsSrI_3 [Fig. 4(c)], the bottom of the valence band region extends from -10.65 to -10.29 eV and is dominated mostly by the I- s like states hybridized with the Sr- p states and the middle of the valence band region which spread from -7.2 eV to -6.9 eV is dominated by the Cs- p like states with very less contribution from I- s states. The topmost region extending from -1.9 to 0 eV is due to the hybridization of the I- p , Sr- d , and Cs- p states (the contribution is less from the Sr and Cs). Conduction band of all the three compounds are dominated by Sr- d states, X ($X = \text{K}, \text{Rb}, \text{and Cs}$)- d states.

Among the three band regions, the lowest band is dominated by K- p states in the case of KSrI_3 , whereas I- s states are present in remaining compounds and the middle region is mainly contributed by the I- s , Rb- p , and Cs- p states for KSrI_3 , RbSrI_3 , and CsSrI_3 compounds, respectively, which is clearly seen in Fig. 4. The top of the valence band is composed mostly of I- p states (less contribution from Sr- s , p , and d states) for all the compounds and this is because of the high electronegativity of iodine when compared to other elements. This again is well explained using the charge density plots in the next section. Bandwidth of the upper valence band region is almost the same for all the compounds under study.

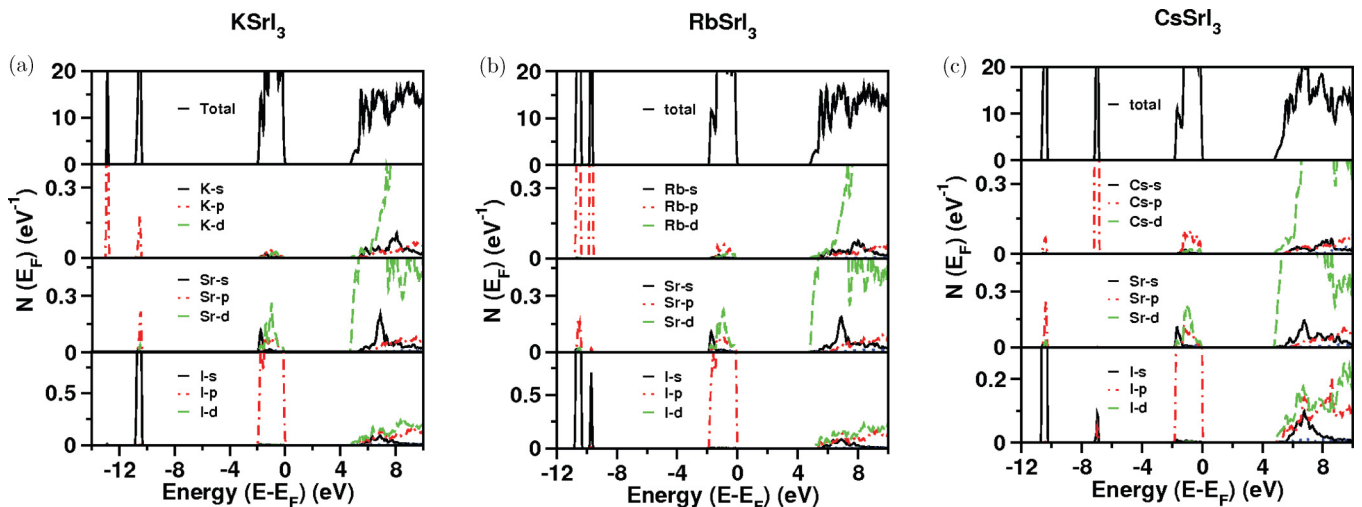


FIG. 4. (Color online) Site projected density of states of KSrI_3 , RbSrI_3 , and CsSrI_3 using TB-mBJ functional.

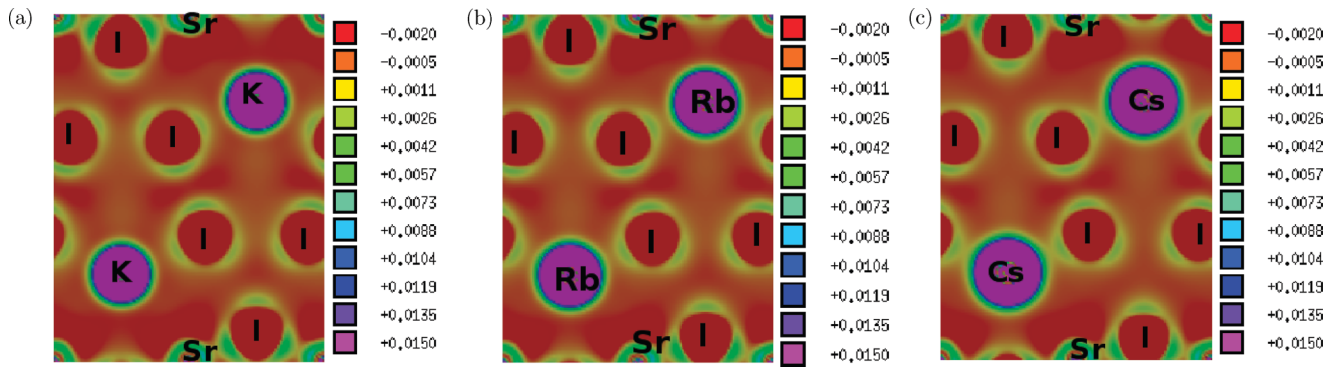


FIG. 5. (Color online) Difference valence electron-density plots of XSrI_3 ($X = \text{K, Rb, Cs}$) in (100) plane using WIEN2k package.

C. Chemical bonding

To analyze the chemical bonding in the investigated compounds [XSrI_3 ($X = \text{K, Rb, Cs}$)], we have plotted the charge density difference plots along (100) plane and are shown in Fig. 5. Due to the higher electronegativity of the iodine (I), compared to the metal atoms X (K, Rb, and Cs) and Sr we observe charge transfer from X , Sr towards the I atoms. This readily reveals the presence of ionic bonding in these materials. In the charge density plots, the presence of isolated atoms indicate the ionic nature of these compounds. Nevertheless, the charge present around the metal atom and the iodine atom mutually share between themselves and the sharing of the charge increases from K to Cs. This indicates that there is also a slight covalent bonding present in these materials and it increases from K to Cs. This fact can also be understood from the DOS plots. From Fig. 4, we can observe hybridization of $I-p$ and $\text{Sr}-d$, p states in the energy region -2 eV to 0 eV (the $I-p$ states are dominant) which clearly indicate the existence of covalent bonding between Sr and I. This hybridization of I and Sr increases from KSrI_3 to CsSrI_3 indicating the increase in the covalent nature as one moves from KSrI_3 to CsSrI_3 .

D. Optical properties

In this section, we discuss the calculated optical properties of the compounds under study using the the TB-mBJ functional. Since optical property calculations need a dense mesh of uniformly distributed k points, we use the $23 \times 23 \times 8$ mesh with 720 k points in the irreducible Brillouin zone (IBZ). The calculated absorptive part ϵ_2 and the dispersive part ϵ_1 of the complex dielectric function $\epsilon(\omega)$ as a function of the photon energy are shown in Fig. 6. The imaginary part of the dielectric function illustrates the optical transition mechanism. The real part ϵ_1 of the dielectric function can be derived from the imaginary part of dielectric function using the Kramers-Kronig relations. The knowledge of both the ϵ_1 and ϵ_2 allows the calculation of important optical functions such as refractive index, reflectivity, and absorption coefficients.

In the imaginary part of complex dielectric function of KSrI_3 as seen in Fig. 6, we find peaks around 6.27 eV, 7.55 eV and the highest energy peak is observed around 21–24 eV region [designated as A_1 , B_1 , and C_1 in Fig. 6(a), lower panel], respectively. The peaks A_1 , B_1 arise mainly due to the transition from $I-p$ states to conduction band (may be

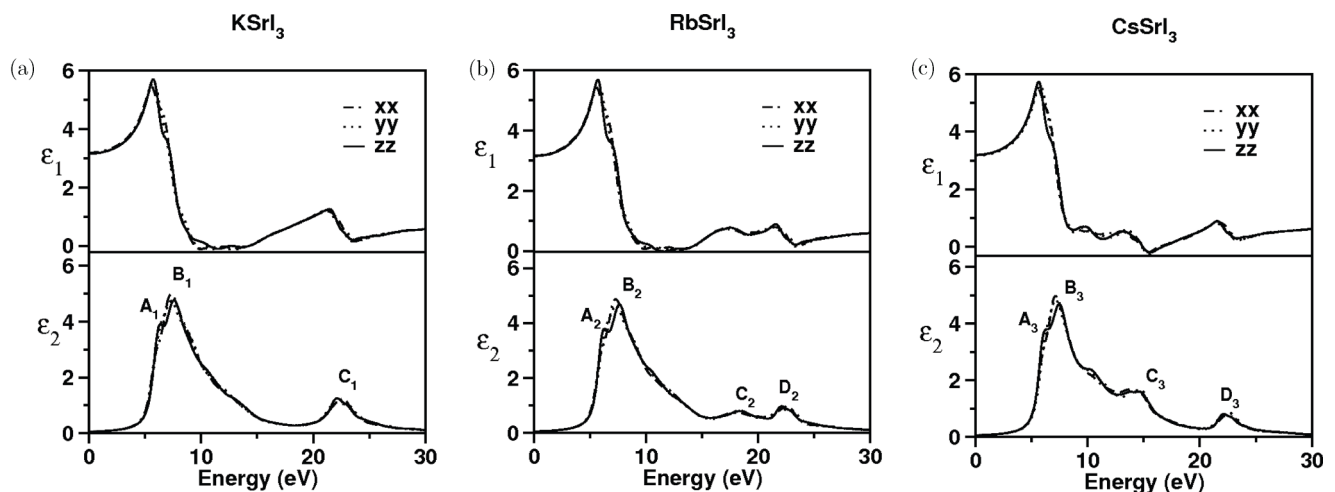
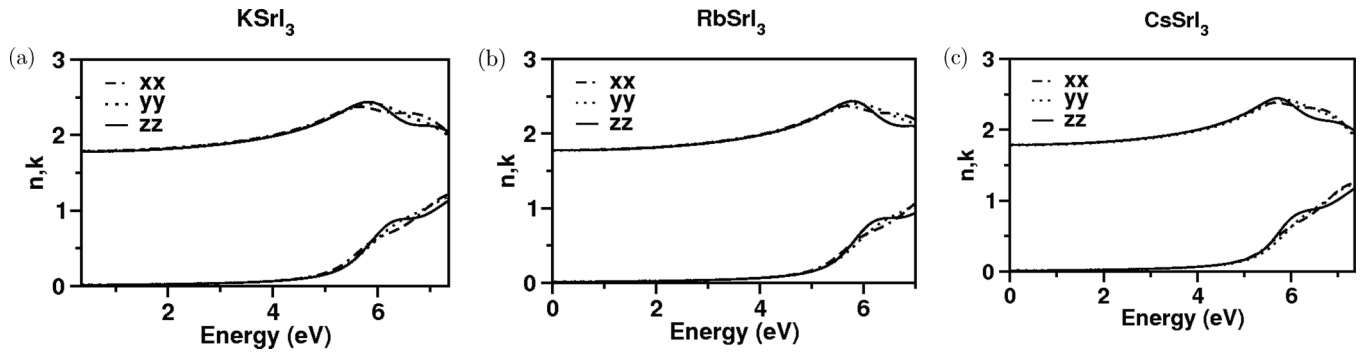


FIG. 6. Real (upper panel) and imaginary (lower panel) parts of dielectric constants KSrI_3 , RbSrI_3 , and CsSrI_3 as calculated with the TB-mBJ functionals.

FIG. 7. Calculated refractive index (n) and extinction coefficients (k).

to the Sr- d and K- d states) and the C_1 peak may be mainly due to the transition from the lower valence level, i.e., from K- p states to higher energy levels of conduction band. The maximum for ϵ_2 is 4.74 is observed at energy 7.55 eV. In the case of RbSrI₃ these peaks are observed at 6.12 eV and 7.56 eV [A_2 , B_2 in Fig. 6(b)] and are due to transition from I- p states to conduction band (may be to the Sr- d and Rb- d states), a broad peak around 15.8–19.58 eV [C_2 in Fig. 6(b)] may be due to the transition from Rb- p to the conduction band, and the high energy peak is at 22 eV which may be due to the transition from I- s states to higher energy levels of conduction band shown as D_2 in Fig. 6(b) and maximum for ϵ_2 is 4.75 around 7.56 eV. In CsSrI₃ the peaks around 6.02 eV and 7.49 eV are due to the transition from I- p states to the conduction band (may be Sr- d and Cs- d states) followed by a broad peak around 12.5–15.81 eV which may be due to the transition from Cs- p to conduction band and peak at 21–23.6 eV arises due to the transition from I- s to higher conduction band levels as shown in Fig. 6(c) and a maximum of 4.67 is observed at 7.5 eV. In all the three compounds, the low energy peaks correspond to transition from I- p states to conduction band, whereas high energy peaks are probably due to transition from lower level valence band (K- p states for K SrI₃, I- s states for RbSrI₃ and CsSrI₃) to the higher energy levels of conduction band. To the best of our knowledge, there are no experimental data available for comparison.

As a next step, we have calculated the refractive index and the same along the three different directions (for all the three compounds) are shown in Fig. 7, which shows the optically isotropic nature of these compounds in the low energy range. For lower energies, refractive index values are almost constant and as the energy increases they attain a maximum value (near the absorption edge) and exhibit decreasing tendency for higher energy values. Refractive index is found to (decrease from K SrI₃ to RbSrI₃ and increase from RbSrI₃ to CsSrI₃) follow an opposite trend to the band gap for all the three compounds (band gap increases from K SrI₃ to RbSrI₃ and decreases from RbSrI₃ to CsSrI₃). A similar trend is also observed in KI, RbI, and CsI compounds.⁵¹ The static refractive index $n(0)$ is found to be around 1.782, 1.777, and 1.786 (average values along the three directions) for X SrI₃ ($X = K, Rb,$ and Cs), respectively. The refractive index along three crystallographic directions, i.e., n_a , n_b , and n_c directions

are given in Table IV. The refractive index reaches a maximum value of 2.43, 2.43, 2.44 at 5.89 eV, 5.80 eV, 5.74 eV for K SrI₃, RbSrI₃, and CsSrI₃ compounds, respectively, which are yet to be compared due to the nonavailability of experimental data.

As mentioned earlier, absorption coefficient of three compounds as a function of photon energy is calculated from the dielectric function (ϵ_1 and ϵ_2) and is shown in Fig. 8, which reveals the manner by which the compounds absorb the incident radiation. Absorption spectra and electronic structure permit basic understanding of scintillating characteristics of materials. The imaginary part of the dielectric spectra is directly proportional to the absorption spectra. In all three compounds, below 5 eV there is no response from these systems which indicate the optical gap of the compounds being around 5 eV. Below this energy range (5 eV) these materials behave like transparent materials. For all the compounds optical absorption spectra is observed in the range of 5–30 eV, i.e., in the ultraviolet region.

The electron energy loss spectra (EELS) represents the motion of the fast electron across the medium that loses an energy per unit length. Prominent features of these spectra is shown in Fig. 9. In K SrI₃ the peaks are observed around 15.36 eV and 24.55 eV, whereas in RbSrI₃ peaks are observed at 14.7 eV, 19.37 eV and high energy peak at around 23.56 eV. In CsSrI₃ these peaks are observed around 12.40 eV (small), 17.71 eV, and 23.57 eV. These prominent peaks in the EELS spectrum are interpreted as plasmon peaks, which denote the electronic charge collective oscillations in the crystal and the corresponding frequencies are called plasma frequencies. Unfortunately, there are no experimental data available to compare our results.

The above investigated compounds are found to be optically isotropic in the low energy region, though they are structurally anisotropic which is the key requirement for the ceramic

TABLE IV. Static refractive index values of K SrI₃, RbSrI₃, and CsSrI₃ along the three crystallographic directions.

	K SrI ₃	RbSrI ₃	CsSrI ₃
n_a	1.787	1.780	1.788
n_b	1.782	1.774	1.781
n_c	1.778	1.776	1.789

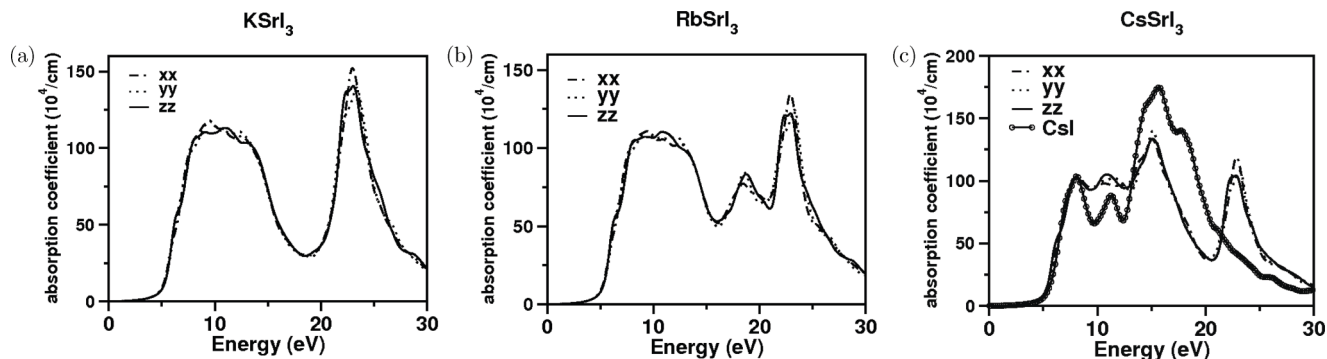


FIG. 8. Absorption spectra of KSrI_3 , RbSrI_3 , and CsSrI_3 (absorption spectra of CsI is inserted in CsSrI_3 plot).

scintillators, but CsSrI_3 is found to be more isotropic in comparison with the other two investigated compounds which is clearly evident from Fig. 7. As discussed earlier in Sec. I, KSrI_3 , RbSrI_3 are of A type, whereas CsSrI_3 is of AL type. When the radiation is incident holes are created in the valence band and electrons are created in the conduction band. In all three compounds, radiative transition is possible by the recombination of holes from the valence band and electron from the conduction band, but in the case of CsSrI_3 the energy difference between core valence band and the valence band is almost equal to the energy gap (AL type), and one can also expect transition of electrons from the valence band to the core valence band which may lead to the fast luminescence in CsSrI_3 . This is compared with the CsI ^{7,8,16,52–55} and is also evident from the absorption spectra of CsI (calculated using WIEN2k package) and CsSrI_3 as shown in Fig. 8, where we observe the absorption peaks of both the compounds to be nearly in the same energy range. Deich *et al.*⁷ observed superfast luminescence and fast luminescence due to transition from $I_{3/2}$ states to $I_{1/2}$ and $I-p$ states to $\text{Cs}-p$ states, respectively. As CsSrI_3 is found to be of AL type, we can also expect fast luminescence in CsSrI_3 , but the splitting of $I-p$ states is not seen with the inclusion of spin-orbit coupling and this could be due to the presence of Sr states in the valence band. So we may not expect any superfast luminescence in CsSrI_3 compound, but we can expect fast luminescence due to the transition from $I-p$ states to $\text{Cs}-p$ states. Emission spectra of the compounds is not analyzed here because present calculation does not describe adequately the excited states in solids. Moreover, Macdonald *et al.*²⁴ also observed

core valence luminescence in CsMgCl_3 , CsSrCl_3 like CsCl which clearly reveals that the presence of additional cation in these compounds weakly influence the valence band formation as most of the cation states are present in the conduction band. Based on the earlier reports and our present calculations, we can expect fast luminescence in CsSrI_3 compound similar to CsI .

IV. CONCLUSIONS

We have studied the $X\text{SrI}_3$ ($X = \text{K}, \text{Rb}, \text{Cs}$) systems with layered structure, where the vdW interactions play a major role in crystal binding and other related properties. To treat vdW interaction in our calculations, we use the OBS correction scheme within PW91 parametrized by GGA as implemented in CASTEP. We investigated the electronic and optical properties of KSrI_3 , RbSrI_3 , and CsSrI_3 compounds with TB-mBJ and compared with the PBE, EV functionals (WIEN2k). We found better improvement of these properties with TB-mBJ functional compared to other functionals. We found these compounds to be indirect band gap materials with VBM at Γ point and CBM at H point. The top of the valence band of all the compounds are dominated by $I-p$ states and conduction band by $\text{Sr}-d$ states and $X(X = \text{K}, \text{Rb}, \text{Cs})-d$ states. The optical transitions are of charge transfer character between metal (alkali, alkaline-earth) derived conduction bands and halogen p -derived valence states. These compounds are found to be optically isotropic though they are structurally anisotropic which cause these materials to be better candidates for the

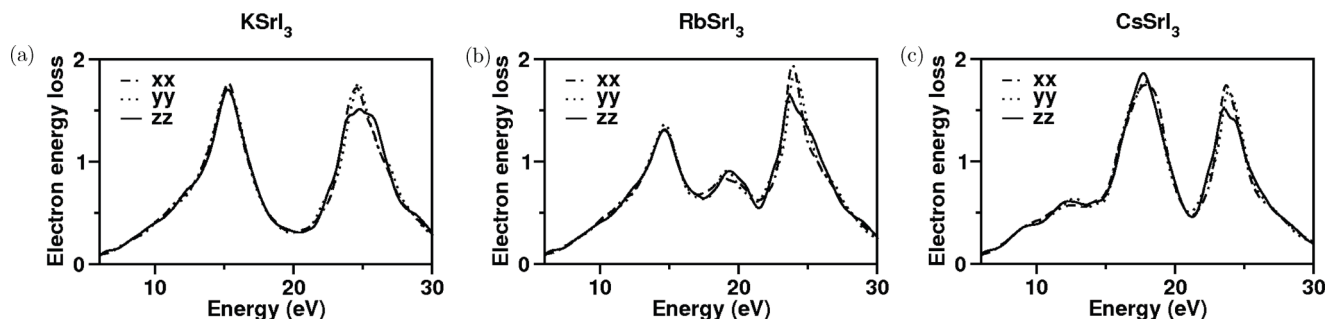


FIG. 9. Electron energy loss function of KSrI_3 , RbSrI_3 , and CsSrI_3 compounds as calculated with TB-mBJ functionals along the three directions.

development as a transparent ceramic scintillators. Among the three compounds studied, we find KSrI_3 and RbSrI_3 to be of A type and CsSrI_3 to be of AL type, which makes CsSrI_3 to be fast scintillating compared to the other compounds under present study.

ACKNOWLEDGMENTS

V.K. would like to acknowledge IIT Hyderabad for the seed grant support. G.S. would like to acknowledge IIT Hyderabad for the fellowship.

*Author to whom correspondence should be addressed: kanchana@iith.ac.in

¹P. Lecoq, A. Annenkov, A. Gektin, M. Korzhik, and C. Pedrini, *Inorganic Scintillators for Detector Systems Physical Principles and Crystal Engineering* (Springer-Verlag, Heidelberg, 2006).

²M. J. Weber, *J. Lumin.* **100**, 35 (2002).

³S. E. Derenzo, M. J. Weber, E. Bourret-Courchesne, and M. K. Klintonberg, *Nucl. Instrum. Methods Phys. Res. A* **505**, 111 (2003).

⁴D. J. Singh, *Phys. Rev. B* **82**, 155145 (2010).

⁵N. Yedukondalu, K. R. Babu, Ch. Bheemalingam, D. J. Singh, G. Vaitheeswaran, and V. Kanchana, *Phys. Rev. B* **83**, 165117 (2011).

⁶P. Schotanus, P. Dorenbos, C. W. E. van Eijk, and R. W. Hollander, *IEEE Trans. Nucl. Sci.* **36**, 132 (1989).

⁷R. Deich, M. Karklina, and L. Nagli, *Solid State Commun.* **71**, 859 (1989).

⁸A. N. Belsky, A. N. Vasil'ev, V. V. Mikhailin, A. V. Gektin, P. Martin, C. Pedrini, and D. Bouttet, *Phys. Rev. B* **49**, 13197 (1994).

⁹E. V. D. van Loef, P. Dorenbos, C. W. E. van Eijk, K. Kramer, and H. U. Gudel, *Appl. Phys. Lett.* **79**, 1573 (2001).

¹⁰D. Aberg, B. Sadigh, and P. Erhart, *Phys. Rev. B* **85**, 125134 (2012).

¹¹D. J. Singh, *Appl. Phys. Lett.* **92**, 201908 (2008).

¹²N. J. Cherepy, G. Hull, A. D. Drobshoff, S. A. Payne, E. van Loef, C. M. Wilson, K. S. Shah, U. N. Roy, A. Burger, L. A. Boatner, W. S. Choong, and W. W. Moses, *Appl. Phys. Lett.* **92**, 083508 (2008).

¹³J. Glodo, E. V. van Loef, N. J. Cherepy, S. A. Payne, and K. S. Shah, *IEEE Trans. Nucl. Sci.* **57**, 1228 (2010).

¹⁴P. A. Rodnyi, *Radiat. Meas.* **33**, 605 (2001).

¹⁵P. A. Rodnyi, *Radiat. Meas.* **38**, 343 (2004).

¹⁶S. Kubota, J. z. Ruan(Gen), M. Itoh, S. Hashimoto, and S. Sakuragi, *Nucl. Instrum. Methods Phys. Res. A* **289**, 253 (1990).

¹⁷A. N. Belsky, I. A. Kamenskikh, V. V. Mikhailin, and A. N. Vasil'ev, *J. Electron Spectrosc. Relat. Phenom.* **79**, 111 (1996).

¹⁸C. W. E. van Eijk, *J. Lumin.* **60**, 936 (1994).

¹⁹S. Zazubovich, *Radiat. Meas.* **33**, 699 (2001).

²⁰A. V. Gektin, *J. Lumin.* **87**, 1283 (2000).

²¹M. Nikl, E. Mihokova, Z. Malkova, A. Vedda, M. Martini, K. Shimamura, and T. Fukuda, *Phys. Rev. B* **66**, 184101 (2002).

²²G. Vaitheeswaran, V. Kanchana, R. S. Kumar, A. L. Cornelius, M. F. Nicol, A. Svane, A. Delin, and B. Johansson, *Phys. Rev. B* **76**, 014107 (2007).

²³M. Fornari, A. Subedi, and D. J. Singh, *Phys. Rev. B* **76**, 214118 (2007).

²⁴M. A. Macdonald, E. N. Melchakov, I. H. Munro, P. A. Rodnyi, and A. S. Voloshinovskiy, *J. Lumin.* **65**, 19 (1995).

²⁵A. N. Belsky, P. Chevallier, E. N. Mel'chakov, C. Pedrini, P. A. Rodnyi, and A. N. Vasil'ev, *Chem. Phys. Lett.* **278**, 369 (1997).

²⁶G. Sanchez-Sanz, L. Seijo, and Z. Barandiaran, *J. Phys. Chem. A* **113**, 12591 (2009).

²⁷M. D. Segall, P. J. D. Lindan, M. J. Probert, C. J. Pickard, P. J. Hasnip, S. J. Clark, and M. C. Payne, *J. Phys.: Condens. Matter.* **14**, 2717 (2002).

²⁸S. J. Clark, M. D. Segall, C. T. Pickard, P. J. Hasnip, M. J. Probert, K. Refson, and M. C. Payne, *Z. Kristallogr.* **220**, 567 (2005).

²⁹M. C. Payne, M. P. Teter, D. C. Allan, T. A. Arias, and J. D. Joannopoulos, *Rev. Mod. Phys.* **64**, 1045 (2002).

³⁰D. Vanderbilt, *Phys. Rev. B* **41**, 7892 (1990).

³¹H. J. Monkhorst and J. D. Pack, *Phys. Rev. B* **13**, 5188 (1976).

³²D. M. Ceperley and B. J. Alder, *Phys. Rev. Lett.* **45**, 566 (1980).

³³J. P. Perdew and A. Zunger, *Phys. Rev. B* **23**, 5048 (1981).

³⁴J. P. Perdew and Y. Wang, *Phys. Rev. B* **45**, 13244 (1992).

³⁵T. H. Fischer and J. Almlof, *J. Phys. Chem.* **96**, 9768 (1992).

³⁶F. Ortman, F. Bechstedt, and W. G. Schmidt, *Phys. Rev. B* **73**, 205101 (2006).

³⁷A. Tkatchenko and M. Scheffler, *Phys. Rev. Lett.* **102**, 073005 (2009).

³⁸S. Grimme, *J. Comput. Chem.* **27**, 1787 (2006).

³⁹S. Grimme, *J. Comput. Chem.* **25**, 1463 (2004).

⁴⁰T. Bucko, J. Hafner, S. Lebegue, and J. G. Angyan, *J. Phys. Chem. A* **114**, 11814 (2010).

⁴¹K. Rapcewicz and N. W. Ashcroft, *Phys. Rev. B* **44**, 4032 (1991).

⁴²H. Ding, K. G. Ray, V. Ozolins, and M. Asta, *Phys. Rev. B* **85**, 012104 (2012).

⁴³P. Blaha, K. Schwarz, P. I. Sorantin, and S. B. Tricky, *Comput. Phys. Commun.* **59**, 399 (1990).

⁴⁴P. Blaha, K. Schwarz, G. K. H. Madsen, D. Kvasnicka, and J. Luitz, WIEN2K, An Augmented plane wave plus Local orbitals Programe for Calculating Crystal Properties, Karlheinz Schwarz, Techn. Universität Wien, Austria, 2001.

⁴⁵J. P. Perdew, K. Burke, and M. Ernzerhof, *Phys. Rev. Lett.* **77**, 3865 (1996).

⁴⁶E. Engel and S. H. Vosko, *Phys. Rev. B* **47**, 13164 (1993).

⁴⁷D. J. Singh, *Phys. Rev. B* **82**, 205102 (2010).

⁴⁸D. Koller, F. Tran, and P. Blaha, *Phys. Rev. B* **83**, 195134 (2011); **85**, 155109 (2012).

⁴⁹F. Tran and P. Blaha, *Phys. Rev. Lett.* **102**, 226401 (2009).

⁵⁰H. Dixit *et al.*, *J. Phys.: Condens. Matter* **24**, 205503 (2012).

⁵¹P. G. Johannsen, *Phys. Rev. B* **55**, 6856 (1997).

⁵²S. Kubota, S. Sakuragi, S. Hashimoto and J.z. Ruan (Gen), *Nucl. Instrum. Methods Phys. Res. A* **268**, 275 (1988).

⁵³M. Abdrakhmanov, S. Chernov, R. Deich, and V. Gavrilov, *J. Lumin.* **54**, 197 (1992).

⁵⁴A. N. Belsky, G. Comtet, G. Dujardin, A. V. Gektin, L. Hellner, I. A. Kamenskikh, P. Martin, V. V. Mikhailin, C. Pedrini, and A. N. Vasil'ev, *J. Electron Spectrosc. Relat. Phenom.* **80**, 109 (1996).

⁵⁵A. N. Belsky, R. Cortes, A. V. Gektin, P. Martin, V. V. Mikhailin, and C. Pedrini, *J. Lumin.* **72**, 93 (1997).

⁵⁶G. Schilling *et al.*, *Z. Anorg. Allg. Chem.* **622**, 759 (1996).